Nitrogen-Doped Carbon Networks for High Energy Density Supercapacitors Derived from Polyaniline Coated Bacterial Cellulose

*Conglai Long, Dongping Qi, Tong Wei, Jun Yan, Lili Jiang, and Zhuangjun Fan**

Bacterial cellulose (BC) is used as both template and precursor for the synthesis of nitrogen-doped carbon networks through the carbonization of polyaniline (PANI) coated BC. The as-obtained carbon networks can act not only as support for obtaining high capacitance electrode materials such as activated carbon (AC) and carbon/MnO_2 hybrid material, but also as conductive networks to integrate active electrode materials. As a result, the as-assembled AC//carbon-MnO_2 asymmetric supercapacitor exhibits a considerably high energy density of 63 Wh kg^{-1} in 1.0 M Na_2SO_4 aqueous solution, higher than most reported AC//MnO_2 asymmetric supercapacitors. More importantly, this asymmetric supercapacitor also exhibits an excellent cycling performance with 92% specific capacitance retention after 5000 cycles. Those results offer a low-cost, eco-friendly design of electrode materials for high-performance supercapacitors.

1. Introduction

Electrochemical capacitors (ECs), also known as supercapacitors, have attracted much attention due to superior power density, fast charge/discharge rates and long cycle lifetime compared to other chemical energy storage devices. However, commercial supercapacitors suffer from low energy density. To meet the increasing energy demands for next-generation ECs, the energy density should be substantially increased without sacrificing the power density and cycle life.[1–5]

Recently, an effective approach to increase the cell voltage is to use asymmetric supercapacitor (ASC) with a Faradaic electrode as energy source (positive electrode) and a capacitive electrode as a power source (negative electrode) in aqueous electrolyte, resulting in a notable improvement of the energy density.[6–8] Much effort has been dedicated to explore various ASC systems, such as graphene-MnO_2//activated carbon nanofiber,[9] $Ni(OH)_2$-graphene//graphene,[10] V_2O_5//activated carbon (AC),[11] $LiMn_2O_4$//AC,[12] RuO_2//AC,[13] and CoAl double-layer hydroxide//AC.[14] Among these hybrid systems, the construction of ASC device using MnO_2 based positive electrode and porous carbon negative electrode is considered as state-of-the-art charge storage technique, providing a high voltage window (up to 2 V), excellent rate performance and good cycling stability.[15,16] However, commercial activated carbon materials often suffer from electrode kinetic problems that are related to inner-pore ion transport, resulting in a poor charge/discharge rate for high-power supercapacitors.[17] By contrast, MnO_2 has attracted intense attention due to its high theoretical pseudo-capacitance, low cost, and environmental compatibility. However, the performances of single-phased MnO_2 are still insufficient to meet growing demands in supercapacitors because of its intrinsic material properties such as low conductivity and poor mechanical stability.[6,18] An advanced approach by incorporating nano-sized MnO_2 with conductive carbon matrix, including carbon nanofoams, carbon nanotubes (CNTs), and graphene, can effectively improve the electrochemical properties of hybrid materials.[9,19–21] Furthermore, the high cost of CNTs and graphene for fabricating supercapacitors should be considered due to their expensive price for widespread commercialization. Given the electrochemical properties and fabrication cost, the selection of carbon materials is important for the construction of both positive and negative materials for ASC applications.[22] Recently there is growing interest for the synthesis of carbon materials derived from biomass precursors owing to their low cost, easy fabrication and environmental compatibility.[23–27] Furthermore, it has been demonstrated that the incorporation of heteroatoms (e.g., nitrogen) into the carbon lattice can significantly enhance the electrical properties of carbon materials, resulting in the enhanced rate capability and cycling performance.[28–30]

Herein, we used bacterial cellulose (BC) as both template and precursor to synthesize N-doped activated carbon (a-CBP) and carbon-MnO_2 hybrid material (c-BP/MnO_2) as the negative and positive electrode materials for ASC device, respectively, as shown in **Scheme 1**. The as-obtained electrode materials have high specific capacitance, short ion diffusion paths and interconnected conductive networks ensuring electron fast transportation throughout the electrode. Consequently, the assembled

Dr. C. L. Long, Dr. D. P. Qi, Prof. T. Wei, Dr. J. Yan, Dr. L. L. Jiang, Prof. Z. J. Fan
Key Laboratory of Superlight Materials and Surface Technology
Ministry of Education
College of Material Science and Chemical Engineering
Harbin Engineering University
Harbin 150001, P. R. China
E-mail: fanzhj666@163.com

DOI: 10.1002/adfm.201304269

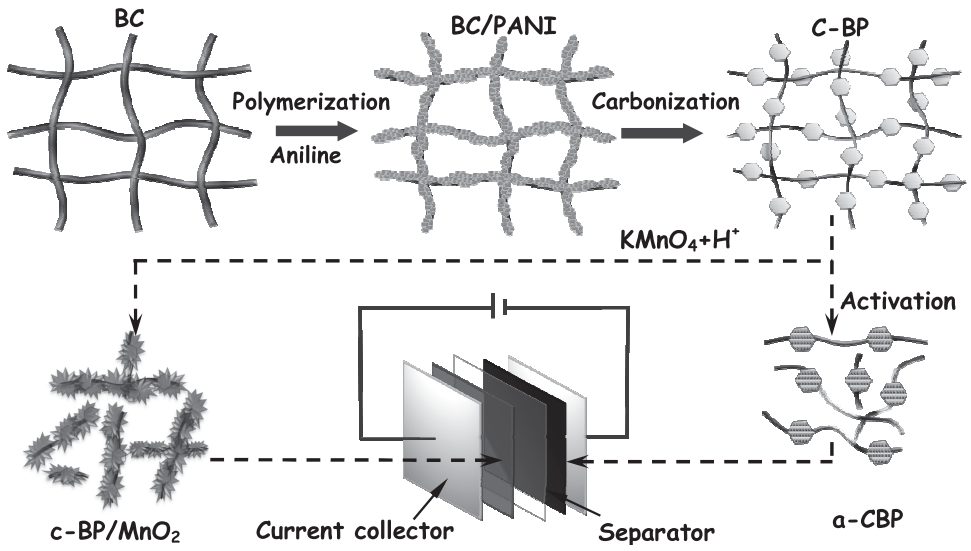

Scheme 1. Schematic diagram illustrating bacterial cellulose (BC) as template and precursor for the synthesis of the electrode materials for asymmetric supercapacitor device.

ASC device can be reversibly charge/discharge at a voltage window of 2.0 V in 1.0 M Na_2SO_4 aqueous solution, obtaining a considerably high energy density of 63 Wh kg^{-1} and maximum power density of 227 kW kg^{-1}. Meanwhile, it is the first time to report that the ASC exhibits excellent cycling stability with 92% capacitance retention after 5000 cycles.

2. Results and Discussion

2.1. Negative Electrode Materials

The BC pellicle (**Figure 1**a) as carbon precursor has three-dimensional interconnected nanofibrous networks with the sizes of 80–100 nm (Figure 1b). After freeze-drying (Figure 1c), lightweight (10 mg cm^{-3}) and flexible BC aerogel retains porous networks structure with numerous intertwined ultrathin nanofibers, providing large surface area and rich hydroxyl (-OH) groups for in-situ polymerization of aniline (Figure 1d) through the strong hydrogen bonding.[31] Scanning electron microscopy (SEM) image of BC/PANI hybrid material (named as BP, Figure 1e) exhibits that PANI is coated onto the interconnected nanofibers via in situ polymerization to form a core-shell structure. X-ray diffraction (XRD) analysis (Supporting Information, Figure S1) confirms that the crystalline structure of BC is partly hindered by the coating of PANI. Moreover, transmission electron microscopy (TEM) image further reveals that PANI coating is made up of randomly orientated small PANI nanosheets that is assembled along the cellulose nanofibers (Figure 1f and Figure S2, Supporting Information), mainly due to strong hydrogen bonding between sequentially formed PANI layer. After the pyrolysis of pure BC, the obtained carbon nanofibers (c-BC) have the diameters of about 10–20 nm and lengths up to several micrometers (Supporting Information, Figure S3). More interestingly, small PANI sheets on BC nanofibers tend to aggregate and form larger dimension sheets due to the accelerated polymerization with increasing temperature, resulting that carbon nanosheets are bridged by the carbon nanofibers (named as c-BP, Figure 1g,h). It is worth noting that porous carbon materials should have sufficiently high surface area, ensuring high energy density for supercapacitors, whereas, narrow pore size distribution with interconnected pore structure and short pore length, are beneficial for the enhanced energy storage capacity and power density. After KOH activation of c-BP (named as a-CBP), porous carbon sheets as energy storage unit are bridged by carbon nanofibers (Figure 1i), and Brunauer-Emmett-Teller (BET) surface area (1326 m^2 g^{-1}) of a-CBP is greatly improved, much higher than those of c-BC (511 m^2 g^{-1}) and c-BP (554 m^2 g^{-1}). Additionally, the pore size distributions of a-CBP and c-BP exhibit that there are more microspores from the chemical activation of carbon sheets (Supporting Information, Figure S4), which greatly enhance the double layer charge storage.

The high-resolution X-ray photoelectron spectroscopy (XPS, Supporting Information, Figure S5) confirms there exists N-containing species (3 atom%) in the as-prepared a-CBP including pyridinic N (N-6, 398 eV), pyrrolic N (N-5, 399.7 eV), quaternary N (N-Q, 400.8 eV) and oxidized N (N-X at 402.5 eV), which can provide electrochemically active sites and good conductivity for the enhanced capacitive properties of the material.[29,32,33] Notably, the percentage of N atoms on the edge of graphite plane (N-5, N-6, and N-X) is 81.9% (Supporting Information, Table S1), much higher than in the middle of graphite plane (N-Q, 18.1%), meaning the existence in more effective active sites.[33] More importantly, nitrogen doping can enhance the surface polarity, electric conductivity, and electron-donor tendency of the carbon materials, which can provide additional pseudo-capacitance, and improve the rate performance and cycling stability for supercapacitors.[28–30] Owing to its porous, N-doped and conductive networks structure, it is expected that a-CBP has an excellent electrochemical performance for supercapacitors.

Electrochemical performance of a-CBP was evaluated in 6 M KOH electrolyte under a three-electrode system, as shown in

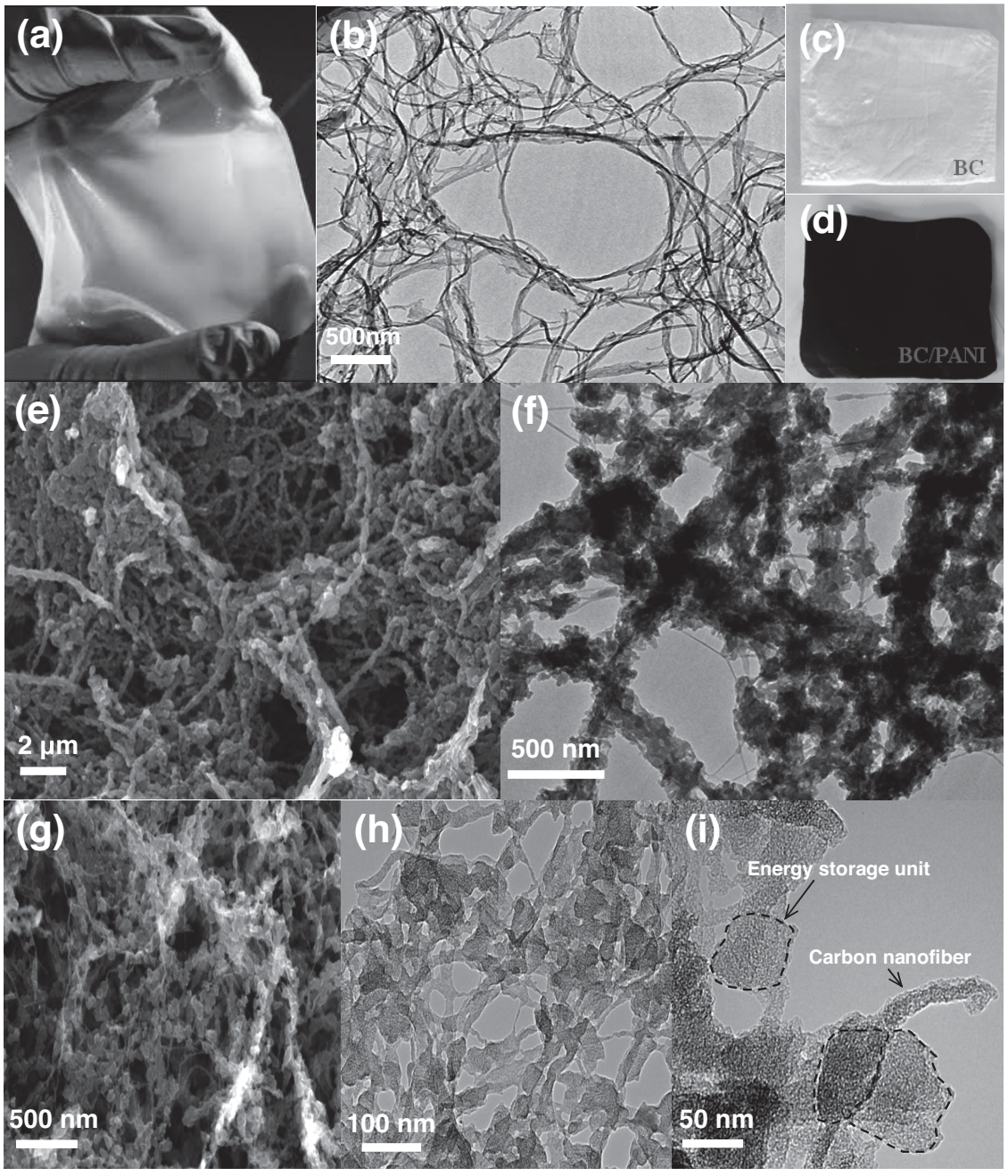

Figure 1. Photographs of a) the pristine material BC pellicle, c) freezing-dired BC, and d) BC/PANI hybrid material. b) TEM image of BC. e) SEM image of BC/PANI. f) TEM image of BC/PANI. g–h) SEM and TEM images of c-BP. i) TEM image of a-CBP.

Figure 2. Due to its excellent conductivity and porous structure, the rectangular shapes of the cyclic voltammogram (CV) curves at scanning rates from 20 to 500 mV s^{-1} are generally retained (Figure 2a), even at high rate of 500 mV s^{-1}, indicating excellent capacitive behaviors. Moreover, the galvanostatic charge/discharge curves of a-CBP electrode (Figure 2b) are highly linear and symmetrical, implying an ideal double layer capacitive characteristic, excellent electrochemical reversibility and charge-discharge properties. Moreover, there is no obvious iR drop for charge/discharge curve even at high current of 20 A g^{-1}, meaning little overall resistance. As shown in Figure 2c, a-CBP has a high specific capacitance of 296 F g^{-1} at 2 mV s^{-1}, much higher than c-BC (161 F g^{-1}) and c-BP (208 F g^{-1}). Significantly, the specific capacitance per unit surface area of a-CBP (22 μF cm^{-2}) is almost twice times higher than that of the commercial carbon Maxsorb (14 μF cm^{-2}).[1] Rate capability is an important factor for the use of supercapacitors in power applications. Notably, a-CBP maintains as high as 221 F g^{-1} at 500 mV s^{-1}, 75% retention at 2 mV s^{-1}, which is much larger than commercial activated carbon (YP17D, Japan) with comparable surface area of 1500 m^2 g^{-1} (127 F g^{-1} at 500 mV s^{-1}, 59% retention at 2 mV s^{-1}, Supporting Information, Figure S6).

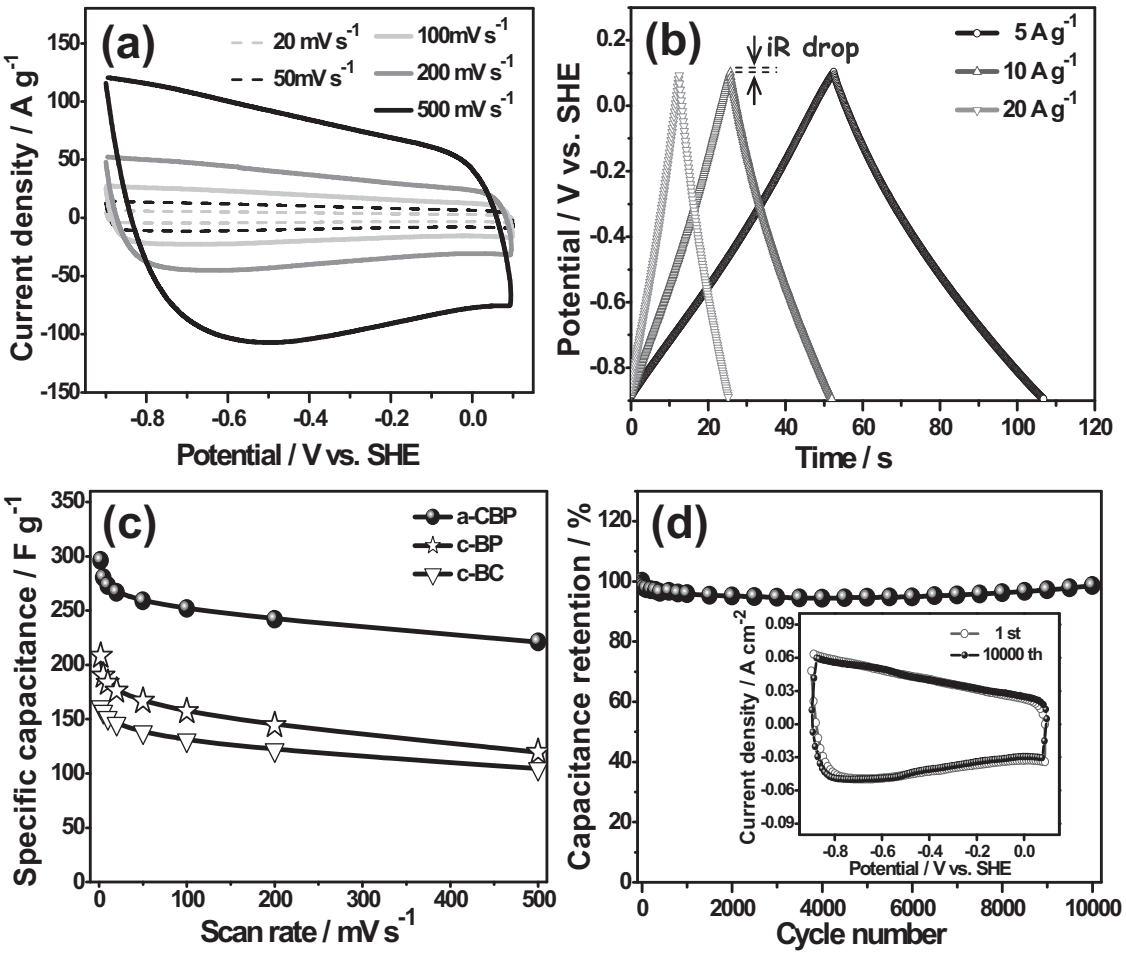

Figure 2. a) CV curves of a-CBP at different scan rates of 20, 50, 100, 200, and 500 mV s^{-1} in 6.0 M KOH electrolyte. b) Galvanostatic charge/discharge curves of a-CBP at different current densities of 5, 10, and 20 A g^{-1}. c) Specific capacitance of a-CBP, c-BP and c-BC electrodes at different scan rates from 2 to 500 mV s^{-1}. d) Cycle performance of a-CBP at a scan rate of 200 mV s^{-1} (the inset shows the CV curves of the 1st and the 10 000th cycle at 200 mV s^{-1}).

Moreover, its rate capability is comparable to those of graphene, activated graphene, and porous carbon nanosphere.[34,35] Clearly, the cycle life of a-CBP was also evaluated at a high scan rate of 200 mV s^{-1} (Figure 2d). After 10 000 cycles, it retains a capacitance retention 99% of initial capacitance, no obvious change for CV curves before and after 10 000 cycles (inset in Figure 2d), demonstrating excellent cycling stability. The excellent rate performance and cycling stability of a-CBP can be ascribed to its unique conductive networks and energy storage units. An interconnected, well-organized 3D conductive network is beneficial for electron transport, and N-doped porous carbon nanosheets with high surface area can provide more active sites for energy storage and shorter ion diffusion length during the charge/discharge process.

2.2. Positive Electrode Materials

Considering that asymmetric supercapacitors with high energy/power density also depend on the electrochemical properties of positive electrode materials, MnO_2 based electrode materials with high capacitance and good rate performance are essential. As known, carbon material can serve as the sacrificial reductant and thereby nanostructured MnO_2 deposits on the carbon matrix, based on the redox reaction between carbon and $KMnO_4$ in acid solution:[36]

$$4KMnO_4 + 3C + 2H_2SO_4 \rightarrow 4MnO_2 + 3CO_2 + 2K_2SO_4 + 2H_2O \quad (1)$$

In this reaction, flower-like MnO_2 is closely anchored on the surface of c-BP (named as c-BP/MnO_2, see **Figure 3**a). Further TEM image confirms that MnO_2 nanosheets are homogeneously distributed throughout the carbon nanosheets and carbon nanofibers (Figure 3b). It is worth noting that MnO_2 nanosheets have the sizes of 200–300 nm and the thickness of 5 nm, the interlayer spacing of MnO_2 crystals is about 0.7 nm (see Figure 3c). More importantly, the scanning transmission electron microscopy (STEM) and X-ray elemental mappings (Figure 3d–g) confirm that the MnO_2 is homogeneously deposited and distributed throughout the c-BP through the spontaneous reduction-deposition process. Additionally, XRD analysis of c-BP/MnO_2 also proves the present of MnO_2 and the obvious diffraction peaks in **Figure 4**a can be assigned to the tetragonal phase of α-type MnO_2 (JCPDS 44–0141).[36,37]

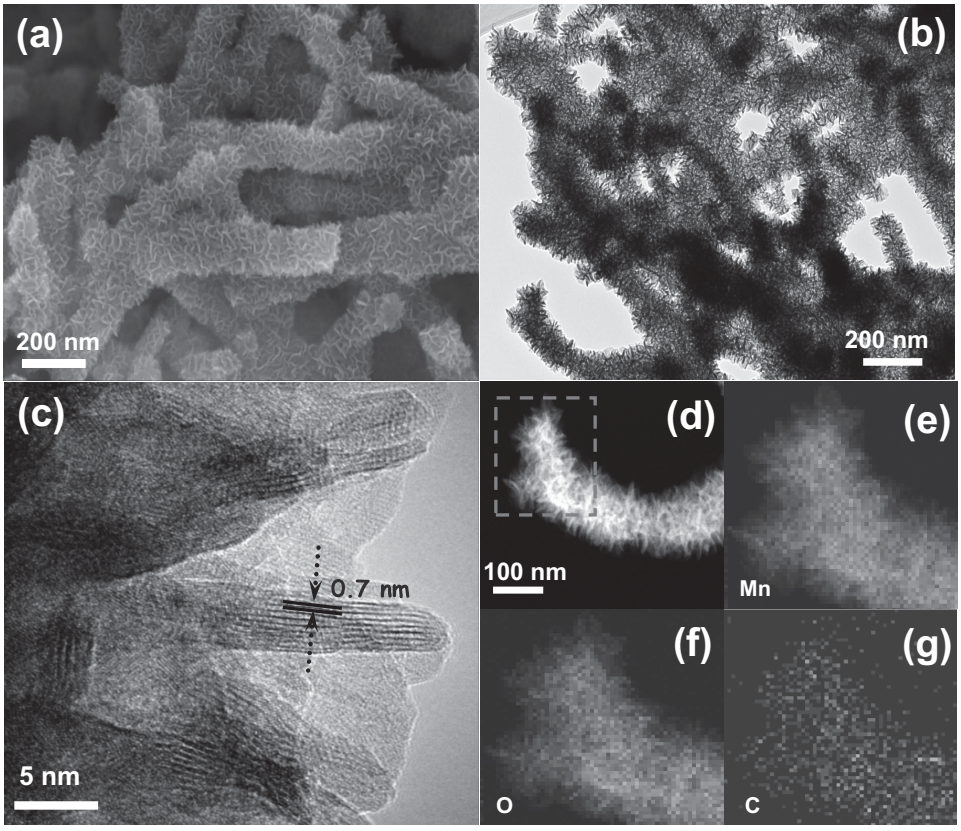

Figure 3. a–b) SEM and TEM images of c-BP/MnO_2. c) High resolution TEM image of c-BP/MnO_2. d–g) STEM images of c-BP/MnO_2 with corresponding elemental mapping images of e) Mn, f) O, and g) C in the dashed square region of (d).

The electrochemical studies for the electrodes were conducted in a three-electrode cell in 1.0 M Na_2SO_4 aqueous electrolyte. For comparison, pure MnO_2 having flower-like structure with a size of 500 nm was also prepared by hydrothermal synthesis method (Supporting Information, Figure S7). Figure 4b shows the CV curves of c-BP/MnO_2 and MnO_2 at 20 mV s^{-1}. Compared with the MnO_2, CV curve of c-BP/MnO_2 is relatively rectangular in shape with near mirror-image current response on voltage reversal, indicating a good reversibility. Also, the galvanostatic charge/discharge curves of c-BP/MnO_2 (Figure 4c) are highly linear and symmetrical, indicating a rapid I–V response and an excellent electrochemical reversibility. Additionally, the specific capacitance of c-BP/MnO_2 is 273 F g^{-1} at 2 mV s^{-1} (Figure 4d), higher than those of pure MnO_2 (190 F g^{-1}) and MnO_2/CNT hybrid material,[20] comparable to MnO_2/graphene hybrid material.[9,21] Notably, the c-BP/MnO_2 electrode shows capacitance retention of 75% at the scan rates from 2 to 100 mV s^{-1}, higher than pure MnO_2 (66%) electrodes. Its excellent rate performance may be attributed from rapid and reversible intercalation/deintercalation of Na^+, or/and adsorption/desorption of H^+ or Na^+ between electrolyte ions and the electroactive material.[21,38] Therefore, the enhanced performance of the c-BP/MnO_2 electrode is attributed to the increased accessible surface area, short ion diffusion length, and fast charge transfer from MnO_2 to carbon substrate *via* conductive carbon networks.

2.3. Asymmetric Hybrid Supercapacitors

As shown in **Figure 5**a, it can be clearly seen that c-BP/MnO_2 and a-CBP electrodes have different voltage windows, and it is expected that the operating cell voltage can be greatly extended when they are assembled into ASC. CV curves of a c-BP/MnO_2//a-CBP ASC device measured at 20 mV s^{-1} with different potential windows in 1.0 M Na_2SO_4 exhibit rectangular-like shapes (Figure 5b) even at the potential window up to 2.0 V, implying an ideal capacitive behavior and a fast charge/discharge property. Significantly, the calculated specific capacitance based on total active electrode mass increases from 75 to 113 F g^{-1} when the operation voltage increases from 1.0 to 2.0 V (Supporting Information, Figure S8). According to the equation of $E = 1/2\ C\ V^2$, the energy density of the ASC is improved by 603%. Moreover, the c-BP/MnO_2//a-CBP ASC device exhibits good rate performance with 53% of capacitance retention when the scan rate increases from 10 to 200 mV s^{-1}.

The excellent performance of ASC device can be ascribed to the following reasons: 1) 3D architecture with MnO_2 sheets grown along carbon nanofibers is beneficial for shortening ion diffusion path, which can greatly reduce the ionic diffusion resistance and charge transfer resistance, resulting in high electrochemical utilization of MnO_2; 2) the excellent interfacial contact between MnO_2 and conductive carbon networks is of great benefit to fast electron transfer throughout the whole electrode matrix; and 3) N-doped porous carbon nanosheets

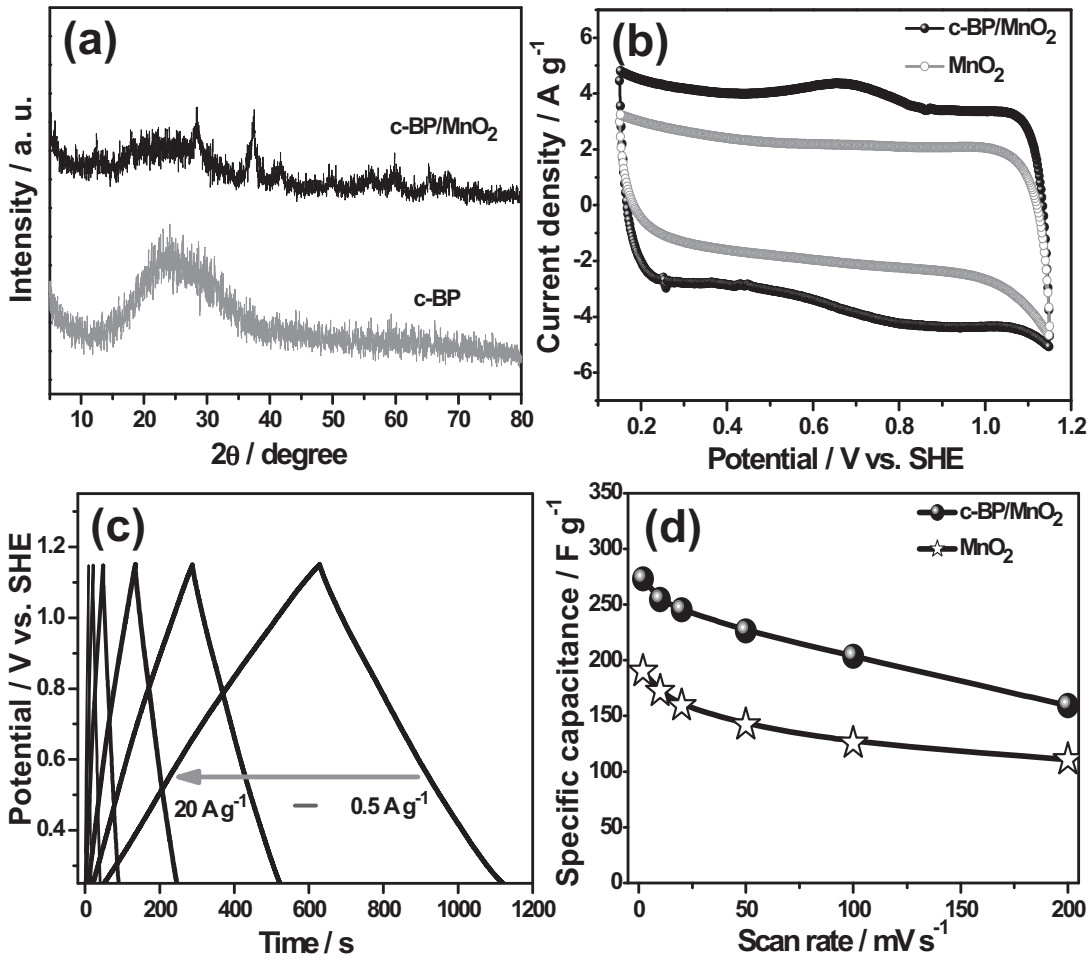

Figure 4. a) XRD patterns of c-BP, c-BP/MnO_2 composite. b) CV curves of c-BP/MnO_2 and MnO_2 at 20 mV s^{-1} in 1.0 M Na_2SO_4 electrolyte. c) Galvanostatic charge/discharge tests of c-BP/MnO_2 at different current densities of 0.5, 1, 2, 5, 10, and 20 A g^{-1}. d) Specific capacitance of c-BP/MnO_2 and MnO_2 at different scan rates.

with high surface area strongly anchored on the interconnected and conductive carbon networks can provide more active sites for energy storage and shorter ion diffusion length during the charge/discharge process. These interesting results pave the way for c-BP/MnO_2//a-CBP ASC device in the development of high-performance electrochemical energy storage devices for practical applications.

The long-term cycling performance of the c-BP/MnO_2//a-CBP ASC device was evaluated in the 2.0 V operating voltage in 1.0 M Na_2SO_4 aqueous electrolyte at 200 mV s^{-1} for 5000 cycles (Figure 5c). It is the first time to report that the asymmetric cell exhibits excellent electrochemical stability with 92% capacitance retention after 5000 cycles. Notably, its cycling performance is comparable to those of other ASCs, such as MnO_2// AC (more than 80% retention after 1500 cycles),[39] MnO_2// AC (93% retention after 100 cycles),[40] MnO_2//AC (53% retention after 50000 cycles),[41] Fe_3O_4//AC (82% retention after 500 cycles),[42] CNTs/MnO_2//CNTs/SnO_2 (92% retention after 1000 cycles),[43] AC//$LiTi_2(PO_4)_3$ (85% retention after 1000 cycles),[44] $Co(OH)_2$//AC (93% retention after 1000 cycles),[45] NiO//AC (50% retention after 1000 cycles),[46] MnO_2//FeOOH (85% retention after 300 cycles),[47] $LiCrTiO_4$//AC (96% retention after 1000 cycles),[48] and MnO_2/MWNT//MWNTs (72% retention after 300 cycles).[49]

Ragone plots of the assembled ASCs (Figure 5d) exhibit the energy density of the c-BP/MnO_2//a-CBP cell at the same power density is much higher than those of MnO_2//a-CBP and MnO_2//c-BP cells. The maximum energy density of the c-BP/MnO_2//a-CBP reaches 63 Wh kg^{-1} at a power density of 227 W kg^{-1}, which is higher than those of MnO_2//a-CBP (40 Wh kg^{-1}), MnO_2//c-BP (36 Wh kg^{-1}) and MnO_2//c-BC (27 Wh kg^{-1}), and still remains 23 Wh kg^{-1} at a power density of 8 kW kg^{-1}. Moreover, the maximum energy density for c-BP/MnO_2//a-CBP cell is much higher than those of symmetrical AC//AC supercapacitors (<10 Wh kg^{-1}),[11,50] CNTs// CNTs supercapacitors (<10 Wh kg^{-1}),[51,52] and MnO_2//MnO_2 supercapacitors (<3.3 Wh kg^{-1}),[53] and MnO_2-based asymmetric supercapacitors with aqueous electrolyte solutions, such as MnO_2//AC (<28.8 Wh kg^{-1}),[40,41,53] $NaMnO_2$//AC (19.5 Wh kg^{-1}),[54] MnO_2//Fe_3O_4 (8.1 Wh kg^{-1}),[53] CNTs/ MnO_2//CNTs/SnO_2 (20.3 Wh kg^{-1}),[43] MnO_2//FeOOH (12 Wh kg^{-1}).[47]

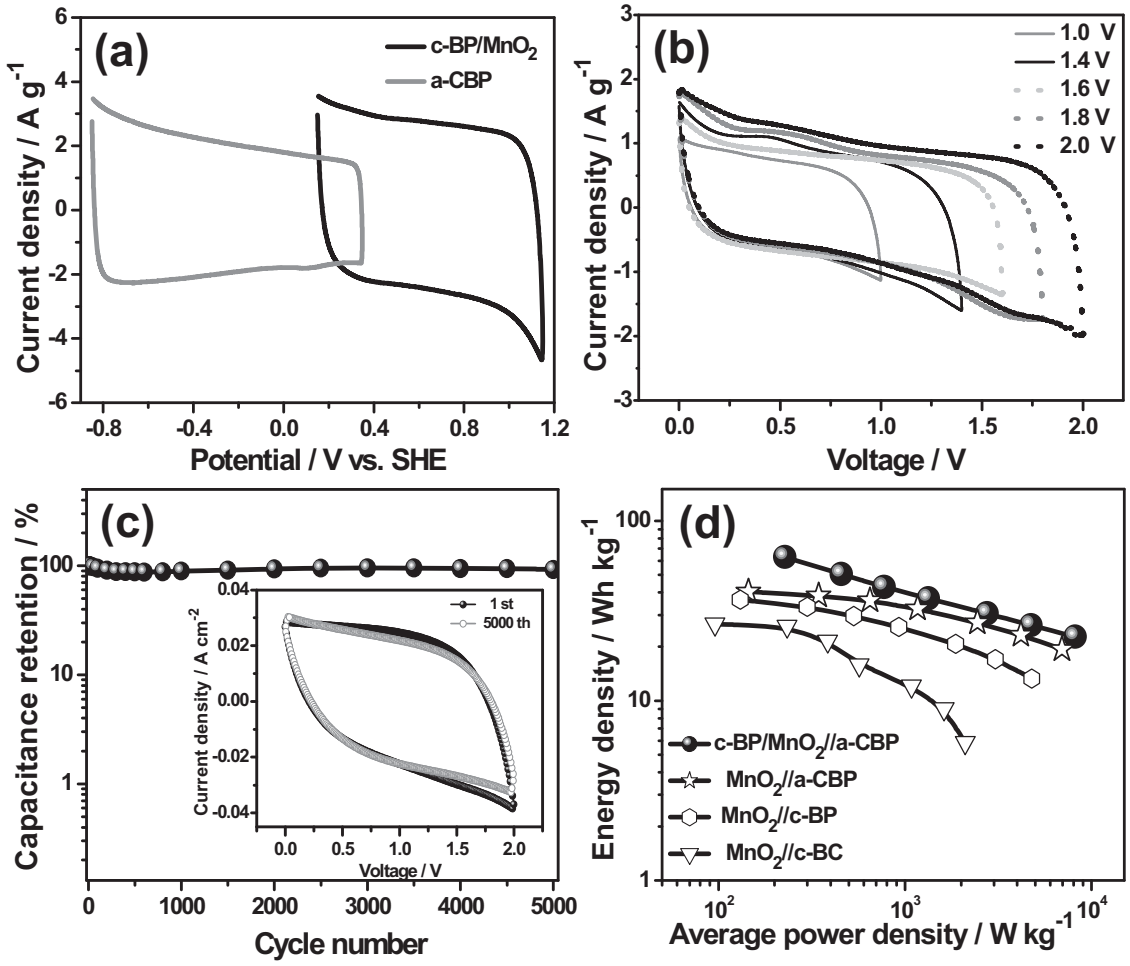

Figure 5. a) Comparative CV curves of a-CBP and c-BP/MnO_2 electrodes performed in a three-electrode cell in 1.0 M Na_2SO_4 aqueous solution at 20 mV s^{-1}. b) CV curves of an optimized c-BP/MnO_2//a-CBP asymmetric supercapacitor measured at different potential windows in 1.0 M Na_2SO_4 aqueous solution at 20 mV s^{-1}. c) Cycle performance of the c-BP/MnO_2//a-CBP asymmetric supercapacitor with a voltage of 2.0 V at 200 mV s^{-1} in 1.0 M Na_2SO_4 aqueous solution (the inset shows the CV curves of the 1st and the 5000th cycle at 200 mV s^{-1}). d) Ragone plots of c-BP/MnO_2//a-CBP, MnO_2//a-CBP, MnO_2//c-BP and MnO_2//c-BC asymmetric cells.

3. Conclusions

In summary, we have demonstrated biomass cellulose as template and precursor for the synthesis of electrode materials for asymmetric supercapacitor device. Nitrogen-doped carbon networks with interconnected and conductive carbon nanofibers can act as support for obtaining high capacitance electrode materials such as activated carbon and MnO_2, as well as providing fast electron transfer throughout the electrode. As a result, the as-assembled asymmetric supercapacitor device with an operation voltage of 2.0 V in 1.0 M Na_2SO_4 aqueous electrolyte delivers a high specific capacitance of 113 F g^{-1}, high energy density of 63 Wh kg^{-1}, and excellent cycling performance (only 8% capacitance loss after 5000 cycles). Therefore, it is a promising strategy for employing low-cost, eco-friendly biomaterials to synthesize advanced electrode materials for high-performance energy storage devices.

4. Experimental Section

Synthesis of BC/PANI Composite Template: The BC pellicles (Hainan Yide Foods Co. Ltd.) were washed by deionized water and freeze-dried in liquid nitrogen. The as-obtained freeze-dried BC (0.7 g) was immersed into aniline hydrochloride solution (0.1 M) for 24 h with stirring at room temperature, enabling the aniline monomers to fully infiltrate through the networks of BC fibers via hydrogen bonding, and cooled to 2 °C in an ice-water bath. Then ammonium persulfate hydrochloride solution (0.125 M) was added dropwise into the above mixture and kept at 0–4 °C for 4 h. Finally, BC/PANI composite was washed with distilled water and ethanol, freeze-dried 24 h, and named as BP.

Synthesis of Negative (a-CBP) and Positive (c-BP/MnO_2) Electrode Materials for Asymmetric Supercapacitor: The BC/PANI composite was carbonized in a crucible within an alumina tube at 850 °C for 2 h under flowing N_2 (99.999%, 200 mL min^{-1}), and the obtained sample was designated as c-BP. For the synthesis of negative electrode material (a-CBP), c-BP and KOH were mixed with a weight ratio of 1:1, heated up to 800 °C and kept for 1 h under flowing N_2. After cooling down to room temperature, the powder was washed repeatedly with 0.5 M HCl

and de-ionized water for several times, and dried at 120 °C overnight. For comparison, BC also was carbonized under the same carbonization procedure, and the obtained sample was named as c-BC.

For the synthesis of positive electrode material (c-BP/MnO_2), c-BP (10 mg) and $KMnO_4$ (100 mg) were added into 10 mL de-ionized water and stirred for 1 h at room temperature. After that, a trace amount of concentrated H_2SO_4 (50 µL, Aldrich, 95–98 wt%) was added into the above mixture and stirred for additional 1 h. Afterwards, the solution was heated in an oil bath at 80 °C for 1 h. The obtained powder was washed repeatedly with de-ionized water for several times, and dried at 120 °C overnight. For comparison, flower-like MnO_2 was synthesized by redox reaction between HCl and $KMnO_4$ without adding carbon under 80–90 °C as described elsewhere.[9]

Characterization: The crystallographic structure of the materials was determined by X-ray diffraction (XRD) equipped with Cu Kα radiation (λ = 0.15406 nm). X-ray photoelectron spectroscopy (XPS) was performed using a PHI5700ESCA spectrometer with a monochromated Al Kα radiation ($h\nu$ = 1486.6 eV); all of the data acquisition and processing were done on XPSPEAK software. The microstructure of the samples was investigated by a field-emission scanning electron microscope (SEM, Camscan Mx2600FE) and transmission electron microscope (TEM, JEOL JEM2010). Pore structure of the samples was characterized by N_2 adsorption at 77 K with a NOVA 2000 (Quantachrome, USA). The specific surface area was calculated by the conventional BET (Brunauer-Emmet-Teller) method. The pore size distributions were analyzed from adsorption branch isotherms by BJH (Barrett-Joyner-Halenda) method.

Electrochemical Characterization: Electrodes used for electrochemical measurements were prepared by mixing electroactive material, carbon black and poly(tetrafluoroethylene) in a mass ratio of 75:20:5 to obtain a slurry. Then the slurry was pressed onto the nickel foam current collector (1 cm × 1 cm) and dried at 100 °C for 12 h. The mass loading of the electrode materials was ~3 mg cm^{-2}. The asymmetric supercapacitor was built with a glassy fibrous separator and performed in a two-electrode cell in 1.0 M Na_2SO_4 aqueous electrolyte solution. The loading mass ratio of positive electrode material and positive electrode material was estimated from the equation as followed:

$$\frac{m_+}{m_-} = \frac{C_- \times V_-}{C_+ \times V_+} \quad (2)$$

Where C is the specific capacitance (F g^{-1}), V is the potential range for the charge/discharge process (V), and m is the mass of the electrode (g).

The electrochemical tests of the individual electrode were performed in a three-electrode cell, in which platinum foil and SCE (or Hg/HgO) electrodes were used as counter and reference electrodes, respectively. Notably, all the values of potential have been normalized to one reference electrode (SHE). All of the above electrochemical measurements were carried out by a CHI 660C electrochemical workstation.

The specific capacitance of the electrode can be calculated according to the following equation:

$$C = \frac{\int I dV}{\upsilon m V} \quad (3)$$

where I is the response current density (A cm^{-2}), V is the potential (V), υ is the potential scan rate (mV s^{-1}), and m is the mass of the electroactive materials in the electrodes (g).

The average power density (P_{av}) was calculated from the equation:

$$P_{av} = \frac{E}{t} \quad (4)$$

where t is the discharge time (s) and E is energy density (J g^{-1}).

Supporting Information

Supporting Information is available from the Wiley Online Library or from the author.

Acknowledgements

The authors acknowledge financial support from the National Science Foundation of China (51077014, 21003028 and 51202043), Fundamental Research funds for the Central Universities, Program for New Century Excellent Talents in University (NCET-10–0050), and Excellent Youth Foundation of Heilongjiang Province of China.

Received: December 23, 2013
Revised: February 1, 2014
Published online: March 18, 2014

[1] P. Simon, Y. Gogotsi, *Acc. Chem. Res.* **2012**, *46*, 1094.
[2] C. Liu, F. Li, L. P. Ma, H. M. Cheng, *Adv. Energy Mater.* **2010**, *22*, E28.
[3] Z. Chen, J. Wen, C. Yan, L. Rice, H. Sohn, M. Shen, M. Cai, B. Dunn, Y. Lu, *Adv. Energy Mater.* **2011**, *1*, 551.
[4] B. Luo, S. Liu, L. Zhi, *Small* **2012**, *8*, 630.
[5] Z. Chen, V. Augustyn, J. Wen, Y. Zhang, M. Shen, B. Dunn, Y. Lu, *Adv. Mater.* **2011**, *23*, 791.
[6] Z. S. Wu, W. Ren, D. W. Wang, F. Li, B. Liu, H. M. Cheng, *ACS Nano* **2010**, *4*, 5835.
[7] C. Long, T. Wei, J. Yan, L. Jiang, Z. Fan, *ACS Nano* **2013**, *7*, 11325.
[8] M. Yang, B. Cheng, H. Song, X. Chen, *Electrochim. Acta* **2010**, *55*, 7021.
[9] Z. Fan, J. Yan, T. Wei, L. Zhi, G. Ning, T. Li, F. Wei, *Adv. Funct. Mater.* **2011**, *21*, 2366.
[10] J. Yan, Z. Fan, W. Sun, G. Ning, T. Wei, Q. Zhang, R. Zhang, L. Zhi, F. Wei, *Adv. Funct. Mater.* **2012**, *22*, 2632.
[11] Q. T. Qu, Y. Shi, L. L. Li, W. L. Guo, Y. P. Wu, H. P. Zhang, S. Y. Guan, R. Holze, *Electrochem. Commun.* **2009**, *11*, 1325.
[12] D. Cericola, P. W. Ruch, R. Kötz, P. Novák, A. Wokaun, *Electrochem. Commun.* **2010**, *12*, 812.
[13] C. C. Hu, K. H. Chang, M. C. Lin, Y. T. Wu, *Nano Lett.* **2006**, *6*, 2690.
[14] Y. G. Wang, L. Cheng, Y. Y. Xia, *J. Power Sources* **2006**, *153*, 191.
[15] J. Zang, X. Li, *J. Mater. Chem.* **2011**, *21*, 10965.
[16] H. Q. Wang, Z. S. Li, Y. G. Huang, Q. Y. Li, X. Y. Wang, *J. Mater. Chem.* **2010**, *20*, 3883.
[17] G. Lota, T. A. Centeno, E. Frackowiak, F. Stoeckli, *Electrochim. Acta* **2008**, *53*, 2210.
[18] A. Sumboja, C. Y. Foo, X. Wang, P. S. Lee, *Adv. Mater.* **2013**, *25*, 2809.
[19] J. Yan, Z. Fan, T. Wei, J. Cheng, B. Shao, K. Wang, L. Song, M. Zhang, *J. Power Sources* **2009**, *194*, 1202.
[20] Z. Fan, M. Xie, X. Jin, J. Yan, T. Wei, *J. Electroanal. Chem.* **2011**, *659*, 191.
[21] J. Yan, Z. Fan, T. Wei, W. Qian, M. Zhang, F. Wei, *Carbon* **2010**, *48*, 3825.
[22] Y. G. Wang, H. Q. Li, Y. Y. Xia, *Adv. Mater.* **2006**, *18*, 2619.
[23] A. Elmouwahidi, Z. Zapata-Benabithe, F. Carrasco-Marin, C. Moreno-Castilla, *Bioresour. Technol.* **2012**, *111*, 185.
[24] Y. J. Kang, S. J. Chun, S. S. Lee, B. Y. Kim, J. H. Kim, H. Chung, S. Y. Lee, W. Kim, *ACS Nano* **2012**, *6*, 6400.
[25] Z. Y. Wu, C. Li, H. W. Liang, J. F. Chen, S. H. Yu, *Angew. Chem. Int. Ed.* **2013**, *52*, 2925.
[26] L. F. Chen, Z. H. Huang, H. W. Liang, Q. F. Guan, S. H. Yu, *Adv. Mater.* **2013**, *25*, 4746.
[27] B. Wang, X. Li, B. Luo, J. Yang, X. Wang, Q. Song, S. Chen, L. Zhi, *Small* **2013**, *9*, 2399.
[28] L. Zhao, Y.-S. Hu, H. Li, Z. Wang, L. Chen, *Adv. Mater.* **2011**, *23*, 1385.
[29] H. Pan, L. Zhao, Y. S. Hu, H. Li, L. Chen, *ChemSusChem* **2012**, *5*, 526.
[30] J. Wei, D. Zhou, Z. Sun, Y. Deng, Y. Xia, D. Zhao, *Adv. Funct. Mater.* **2013**, *23*, 2322.

[31] H. Wang, E. Zhu, J. Yang, P. Zhou, D. Sun, W. Tang, *J. Phys. Chem. C* **2012**, *116*, 13013.
[32] Z. Li, L. Zhang, B. S. Amirkhiz, X. Tan, Z. Xu, H. Wang, B. C. Olsen, C. M. B. Holt, D. Mitlin, *Adv. Energy Mater.* **2012**, *2*, 431.
[33] S. Biniak, G. Szymanski, J. Siedlewski, A. Swiatkowski, *Carbon* **1997**, *35*, 1799.
[34] S. Murali, J. R. Potts, S. Stoller, J. Park, M.D. Stoller, L. L. Zhang, Y. Zhu, R. S. Ruoff, *Carbon* **2012**, *50*, 3482.
[35] F. Su, C. K. Poh, J. S. Chen, G. Xu, D. Wang, Q. Li, J. Lin, X. W. Lou, *Energy Environ. Sci.* **2011**, *4*, 717.
[36] Y. Chen, Y. Zhang, D. Geng, R. Li, H. Hong, J. Chen, X. Sun, *Carbon* **2011**, *49*, 4434.
[37] W. Xiao, D. Wang, X. W. Lou, *J. Phys. Chem. C* **2009**, *114*, 1694.
[38] H. Pan, Y.-S. Hu, L. Chen, *Energy Environ. Sci.* **2013**, *6*, 2338.
[39] A. Yuan, Q. Zhang, *Electrochem. Commun.* **2006**, *8*, 1173.
[40] M. S. Hong, S. H. Lee, S. W. Kim, *Electrochem. Solid-State Lett.* **2002**, *5*, A227.
[41] T. Brousse, P. L. Taberna, O. Crosnier, R. Dugas, P. Guillemet, Y. Scudeller, Y. Zhou, F. Favier, D. Bélanger, P. Simon, *J. Power Sources* **2007**, *173*, 633.
[42] X. Du, C. Wang, M. Chen, Y. Jiao, J. Wang, *J. Phys. Chem. C* **2009**, *113*, 2643.
[43] C. Yu, C. Masarapu, J. Rong, B. Wei, H. Jiang, *Adv. Mater.* **2009**, *21*, 4793.
[44] J. Y. Luo, Y. Y. Xia, *J. Power Sources* **2009**, *186*, 224.
[45] L. B. Kong, M. Liu, J. W. Lang, Y. C. Luo, L. Kang, *J. Electrochem. Soc.* **2009**, *156*, A1000.
[46] D. W. Wang, F. Li, H. M. Cheng, *J. Power Sources* **2008**, *185*, 1563.
[47] W. H. Jin, G. T. Cao, J. Y. Sun, *J. Power Sources* **2008**, *175*, 686.
[48] C. V. Rao, B. Rambabu, *Solid State Ionics* **2010**, *181*, 839.
[49] G. X. Wang, B. L. Zhang, Z. L. Yu, M. Z. Qu, *Solid State Ionics* **2005**, *176*, 1169.
[50] D. W. Wang, F. Li, M. Liu, G. Q. Lu, H. M. Cheng, *Angew. Chem. Int. Ed.* **2008**, *47*, 373.
[51] K. H. An, W. S. Kim, Y. S. Park, J. M. Moon, D. J. Bae, S. C. Lim, Y. S. Lee, Y. H. Lee, *Adv. Funct. Mater.* **2001**, *11*, 387.
[52] M. Kaempgen, C. K. Chan, J. Ma, Y. Cui, G. Gruner, *Nano Lett.* **2009**, *9*, 1872.
[53] T. Cottineau, M. Toupin, T. Delahaye, T. Brousse, D. Bélanger, *Appl. Phys. A* **2006**, *82*, 599.
[54] Q. T. Qu, Y. Shi, S. Tian, Y. H. Chen, Y. P. Wu, R. Holze, *J. Power Sources* **2009**, *194*, 1222.